FEMS Microbes, 2026, **7**, xtag011
https://doi.org/10.1093/femsmc/xtag011
Published: 20 February 2026
Research article – Microbes & Metabolism

Crystal structure of methanogen MtxX (Methanogen Marker Protein MMP4) from *Methanothermobacter thermautotrophicus* ΔH

Andrew J. Sutherland-Smith [1,*], Vincenzo Carbone [2,*], Wiebke Kaziur-Cegla [2], Marion Woermann [2], Linley R. Schofield [2], Ron S. Ronimus [2]

[1]School of Food Technology and Natural Sciences, Massey University, Palmerston North 4442, New Zealand
[2]AgResearch Group, Bioeconomy Science Institute, Palmerston North 4442, New Zealand
*Corresponding authors. Andrew J.Sutherland-Smith, School of Food Technology and Natural Sciences, Massey University, Palmerston North, 4442, New Zealand. E-mail: a.j.sutherland-smith@massey.ac.nz; Vincenzo Carbone, AgResearch Group, Bioeconomy Science Institute, Palmerston North, 4442, New Zealand. E-mail: vince.carbone@agresearch.co.nz
Editor: Biswarup Mukhopadhyay

Abstract

MtxX, also known as Methanogen Marker Protein 4 (MMP4), is a member of the group of proteins conserved in archaeal methanogens called the Methanogen Marker Proteins (MMPs). Owing to this taxonomic distribution the MMPs are presumed to have roles related to methanogenesis or are evidence for an evolutionary history associated with methanogenic processes. MtxX is sequence-annotated as either a methyltransferase (EC 2.1.1.-) or a phosphate acetyl/butyryltransferase (EC 2.3.1.8/2.3.1.19). Gene synteny analysis shows *mtxX* is located next to other MMP genes in Methanomicrobiales, Methanotrichales, and Methanocaldococcus genomes, while in Methanobacteria and Methanococci it is positioned adjacent to undecaprenyl pyrophosphate synthase, a cell wall biosynthesis enzyme. We describe the crystal structure for MtxX from *Methanothermobacter thermautotrophicus* ΔH showing that it has a protein fold homologous to phosphate acetyltransferases and decarboxylating NAD(P)-dependent dehydrogenases. The MtxX structure has a conserved binding cleft which is the presumptive functional site based on crystallographic symmetry-related molecular binding interactions and structural homology.

Keywords MtxX, MMP4, archaea, methanogen, Methanogen Marker Protein 4, *Methanothermobacter thermautotrophicus* ΔH

Introduction

MtxX, also known as Methanogen Marker Protein 4, is a member of the group of proteins identified as being almost unique to methanogenic archaea (Basu et al. 2011), and hence has been proposed to play a functional role in methanogen-unique pathways, being either directly or indirectly involved in methanogenesis (Gao and Gupta 2007, Leahy et al. 2010, Kaster et al. 2011, Wang et al. 2015, Borrel et al. 2019, Adler et al. 2025). *mtxX* is included in a set of core methanogenesis genes defined as being present in more than 90% of sequenced methanogens and less than 5% of other sequenced non-methanogenic archaea (Borrel et al. 2014). *mtxX* is present in class I/II methanogens, the anaerobic methanotrophic (ANME) Methanosarcinales and Syntrophoarchaeales, and the methyl-dependent hydrogenotrophic methanogens, such as Methanomassiliicoccales and Methanofastidiosales (Wang et al. 2015, Nobu et al. 2016, Borrel et al. 2019). Whole-genome transposon insertion mutagenesis in *Methanococcus maripaludis* S2 indicated *mtxX* is possibly essential (Sarmiento et al. 2013). However, *mtxX* is also present in some archaeal genomes that do not contain methyl coenzyme-M reductase (MCR) or *mcr*-like genes, for example some Archaeoglobales and Promethearchaeaceae, raising the possibility that MtxX is a remnant of a methane-associated metabolism that has diverged in function (Borrel et al. 2019, Adam et al. 2022). For Methanosarcinales *mtxX* is co-located in an operon with *mtxA* and *mtxH* which are predicted homologues of MtrA and MtrH (Harms and Thauer 1997, Wang et al. 2015). Cobalamin-binding MtrA, and MtrH are subunits of the membrane-bound methyltransferase (Mtr) that transfers a methyl group from methyl-H_4MPT to coenzyme M, a reaction coupled to Na^+ gradient generation (Harms et al. 1995). However, MtrA and MtrH are not conserved for all methanogens and are also not restricted to methanogens, being found in other archaea and bacteria (Wang et al. 2015, Adam et al. 2022).

A specific function for MtxX remains unresolved. Based on its co-localization with *mtxA* and *mtxH* in some genomes, *mtxX* has been annotated as a methyltransferase or methyltransferase related protein. For example, *Methanothermobacter thermautotrophicus* ΔH MtxX (*Mth*MtxX) UNIPROT O26333 is annotated as an uncharacterized methyltransferase (EC 2.1.1.-). However, sequence-based homology indicates closer similarity for MtxX sequences to phosphate acetyl/butyryltransferases (phosphotransacetylases)

Received: 11 September 2025. **Revised:** 10 February 2026. **Accepted:** 13 February 2026

Table 1 *Mth*MtxX crystal, data collection and refinement parameters.

	Native	**0.5 M Sodium iodide soak**
Space group	$P2_1$	$P2_1$
Unit cell parameters:		
a, b, c (Å)	56.48 72.31 65.58	56.57 72.42 65.37
α, β, γ (°)	90.00 96.12 90.00	90.00 96.10 90.00
Wavelength (Å)	0.95365	0.95372
Resolution Range (Å)	65.21–1.60 (1.63–1.60)	38.28–1.68 (1.71–1.68)
No. of observed reflections	435 174 (14 654)	409 955 (16 098)
No. of unique reflections	69 258 (3397)	59 821 (2784)
R_{meas}	0.071 (1.00)	0.061 (0.75)
R_{pim}	0.027 (0.48)	0.023 (0.31)
$CC_{1/2}$	1.00 (0.78)	1.00 (0.84)
Completeness (%)	100.0 (99.6)	99.4 (91.1)
Multiplicity	6.3 (4.3)	6.9 (5.8)
$I/\sigma(I)$	15.4 (1.0)	13.8 (1.8)
Refinement parameters:		
Resolution range (Å)	65.3–1.6	
Number of reflections, refined	69 236	
Number of reflections, R free	3507	
R factor	0.163	
R free	0.185	
RMSD bond lengths (Å)	0.0095	
RMSD bond angles (°)	1.72	
Ramachandran plot:		
Favoured regions (%)	99	
Allowed regions (%)	1	
Outliers (%)	0	

Parameters for data in the highest resolution shell are given in parentheses

(EC 2.3.1.8/19) (Harms and Thauer 1997, Shin 2008, Adam et al. 2022), and for many methanogen genomes *mtxX* is found outside any recognized methanogenesis-specific transcriptional unit, as is the case for *M. thermautotrophicus* ΔH. As a step in defining the role of MtxX in methanogens we have analyzed *mtxX* gene synteny and determined the first X-ray crystal structure of MtxX.

Materials and methods

mtxX gene synteny analysis was performed for methanogen classes Methanobacteria (49 genomes), Methanopyri (3 genomes), Methanococci (19 genomes), Methanomicrobia (98 genomes), and Methanomassiliicoccocales (7 genomes) using SyntTax (Oberto 2013), and with the MtxX protein sequence using BLASTP searches of Archaea. Organism name and taxonomic lineage were defined according to the NCBI Taxonomy database (Federhen 2012).

The *Mth*MtxX DNA sequence (MTH_231, 1470192) was PCR subcloned into the pET151D vector for *E. coli* heterologous expression as a 6xHis-tagged protein. Transformed *E. coli* BL21(DE3) cells were grown at 37°C in 2xYT/100 μg/ml ampicillin to a cell density OD_{600} of 0.4–0.55 when expression was induced by the addition of isopropyl-β-D-1-thiogalactopyranoside to a concentration of 1 mM. The cultures were incubated with shaking at 25°C for overnight expression, and the cells harvested by centrifugation and frozen. For MtxX purification, the cells were thawed-refrozen for three cycles before lysozyme (final concentration 1 mg/ml) treatment to ensure lysis. DNase and RNase (final concentrations 5 μg/ml), 7 mM β-mercaptoethanol and 0.5 mM phenylmethanesulfonyl fluoride were added to the cell lysate in equilibration buffer 50 mM Tris, 10 mM imidazole, 20 mM $MgCl_2$ and 300 mM NaCl at a ratio of 5 ml buffer per g of cell pellet. The cell lysate was filtered using a 0.22 μm Millex GP filter unit (Merck Millipore Ltd., Ireland) and applied to a Ni^{2+} Sepharose-6 Fast Flow column pre-rinsed in equilibration buffer. After the cell lysate was applied to the column, the unbound lysate fraction was removed by washing with equilibration buffer, followed by elution of MtxX by the addition of elution buffer (50 mM Tris, 250 mM imidazole, 20 mM $MgCl_2$, 300 mM NaCl). The protein concentration was measured by Bradford assay and the protein purity analyzed by SDS-PAGE. MtxX was concentrated to 4 mg/ml and buffer exchanged into 20 mM MOPS pH 7, 2 mM tris(2-carboxyethyl)phosphine, 500 mM KCl and 10% (v/v) glycerol.

MtxX (filtered through a 0.22 μm membrane) was crystallized from 0.1 M Na HEPES pH 7.5, 10% (w/v) PEG 8000, 8% (v/v) ethylene glycol (Molecular Dimensions Structure Screen 2 #19) using sitting drop vapour diffusion at 21°C in a vibration free incubator. A native X-ray diffraction dataset (Table 1) was collected on a MtxX crystal soaked in mother liquor supplemented with 1 mM $SrCl_2$ and frozen in the presence of 25% (w/v) ethylene glycol at the Australian Synchrotron beamline MX1 (Cowieson et al. 2015). The crystal was found to exhibit $P2_1$ symmetry with unit cell dimensions 56.5 72.3 65.6 Å, 90, 96.1, 90° indicating two molecules in the asymmetric unit. Butyric acid was tested as a potential

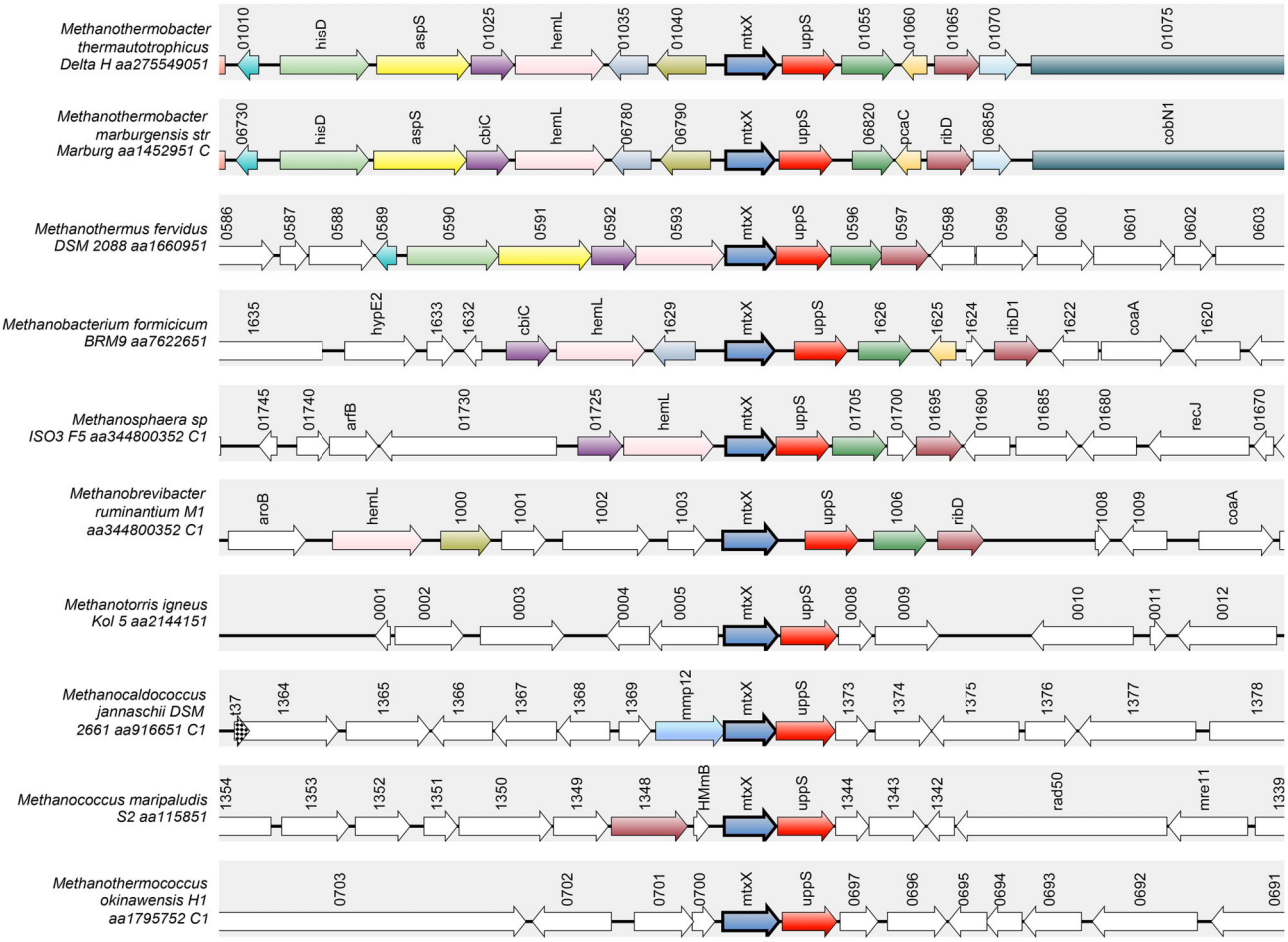

Figure 1 Representation of *mtxX* gene synteny from a subset ($n = 10$) of the analyzed Methanobacteria and Methanococci genomes. Annotated *M. thermautotrophicus* ΔH genes (left to right): *hisD* (light green) histinol dehydrogenase GenBank accession WBF06543.1. *aspS* (yellow) aspartate tRNA ligase WBF06544.1. 01025/*cbiC* (purple) cobalt-recorrin 8 methylmutase WBF06545.1. *hemL* (pink) glutamate-1-semialdehyde 2,1-aminomutase WBF06546.1. *mtxX* (dark blue and bold outline) methanogen markerprotein 4 WBF06549.1. *uppS* (red) di-trans, poly-cis-decaprenylcistransferase WBF06550.1. 01055 (green) Tat family hydrolase WBF07186.1. 01060 (beige) carboxymuconolactone decarboxylase WBF06551.1. 01075/*cobN1* (grey–blue) cobaltochelatase subunit CobN WBF06554.1. *Methanocaldococcus jannaschii* Methanogen Marker Protein 12 *mmp12* is shaded light blue. The figure was prepared from SyntTax (Oberto 2013).

MtxX ligand in crystal soaking experiments but does not show binding.

Structure determination

The MtxX structure was determined using the SIRAS method from X-ray diffraction data collected on a 0.5 M NaI soaked MtxX crystal, grown in the conditions above, at the Australian Synchrotron MX2 beamline (Aragao et al. 2018). Native and derivative diffraction data were integrated using DIALS (Winter et al. 2018) and XDS (Kabsch 2010), followed by merging and averaging the intensities with POINTLESS/AIMLESS (Evans 2011, Evans and Murshudov 2013). The MtxX crystal structure was determined using SHELX-C/D/E (Sheldrick 2010) as implemented in the CRANK2 (Skubak and Pannu 2013) pipeline accessed via CCP4 (Winn et al. 2011). SHELX located six iodide sites with occupancy greater than 0.25, resulting in a substructure determination with a combined figure of merit of 0.21, with subsequent model building yielding a correlation coefficient of 49.5. Density modification and automated building with Buccaneer (Cowtan 2006), and REFMAC5 refinement (Murshudov et al. 2011) produced a near complete structure (450 amino acids, 93%) for the two MtxX molecules in the asymmetric unit, with R/Rfree 0.23/0.26. Further cycles of combined manual rebuilding in Coot (Emsley and Cowtan 2004) and refinement using REFMAC5 improved the structure further. Local non-crystallographic symmetry restraints were used during refinement except for the final cycles of refinement. Structure stereochemistry validation with MOLPROBITY (Davis et al. 2004) shows 99% amino acids in the favoured regions of the Ramachandran plot and no outliers. Deviations from ideal stereochemistry for the MtxX structure are better than typical for the resolution of the diffraction data (Table 1). The structure contains molecule A of residues 7–242 (C-terminus), molecule B 8–235, 283 solvent molecules and one ethylene glycol molecule with R factor and Rfree of 0.163 and 0.185 (5% reflections), respectively. Overall, the electron density is well defined except for the N-terminal 40 residues of molecule B which have weaker density. The MtxX atomic coordinates and structure factors have been deposited in the RCSB protein data bank with

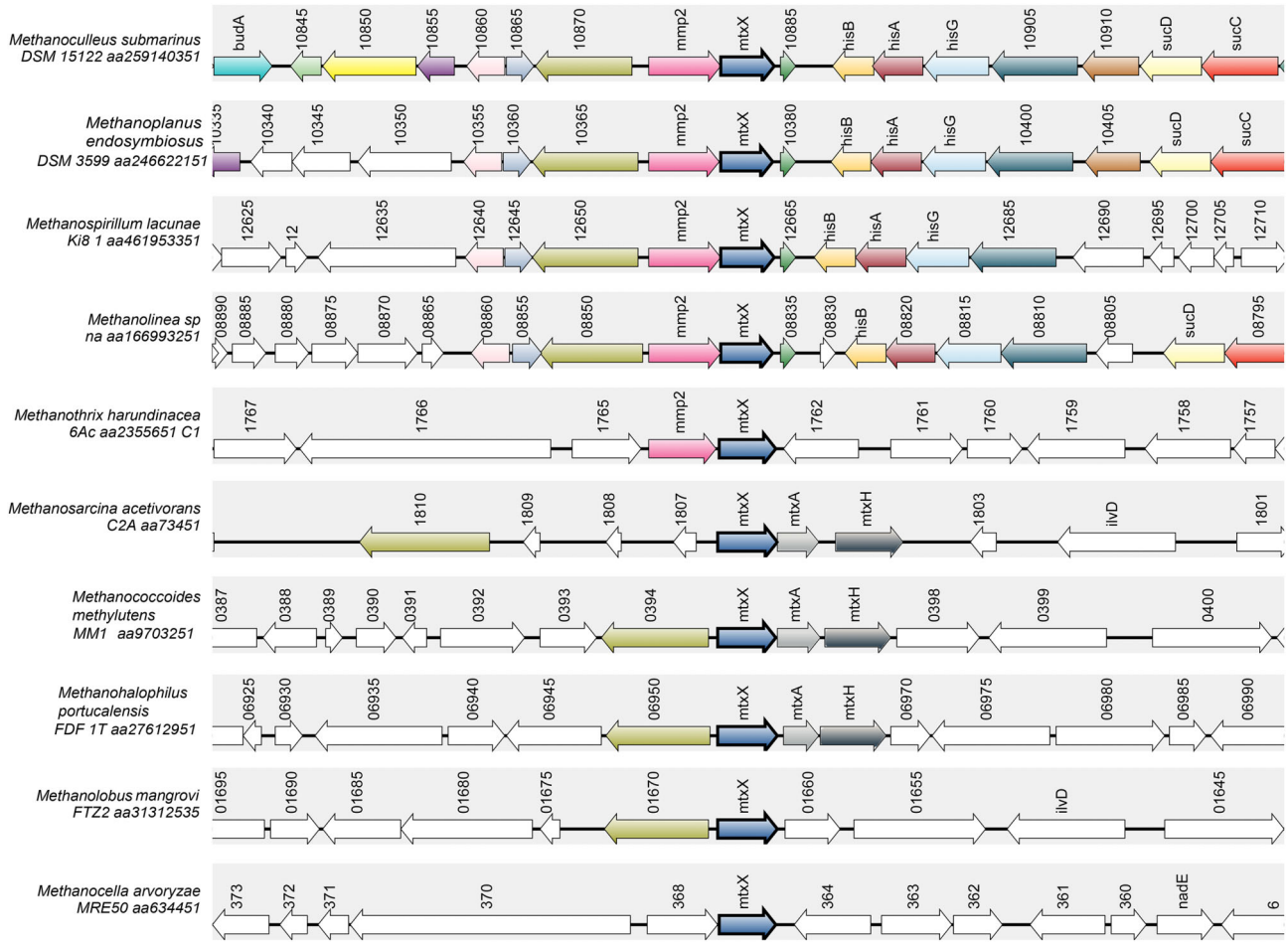

Figure 2 Representation of *mtxX* gene synteny from a subset ($n = 10$) of the analyzed Methanomicrobia genomes. *Methanoculleus submarinus* annotated genes from left to right. 10855 (purple) universal stress protein GenBank accession UYU18191.1. 10860 (pink) archaemetzincin family Zn-dependent metalloprotease UYU18192.1. 10870 (olive) replication factor C large subunit UYU18194.1. *mmp2* (10875) (pink) Methanogen Marker Protein 2 UYU18195.1. *mtxX* (dark blue and bold outline) methanogen marker protein 4 UYU18196.1. 10885 (green) histone family protein UYU18197.1. *hisB* (orange) imidazoleglycerol-phosphate dehydratase UYU18198.1. *hisA* (red-brown) 1-(5-phosphoribosyl)-5-[(5phosphoribosylamino)methylideneamino] imidazole-4-carboxamide isomerase UYU18199.1. *hisG* (cyan) ATP phosphoribosyltransferase UYU18200.1. 10905 (grey-blue) methionine adenosyltransferase UYU18201.1. 10910 (brown) diadenylate cyclase UYU18202.1. *sucD* (yellow) succinate-CoA ligase subunit alpha UYU18203.1. 10920/*sucC* (red) acetate-CoA ligase family protein UYU18204.1. *Methanosarcinia acetivorens*, *Methanococcoides methylutens*, and *Methanohalophilus portucalensis mtxA* and *mtxH* are shaded light grey and dark grey respectively. The figure was prepared from SyntTax (Oberto 2013).

code 9NZY. Structural figures were prepared with CCP4mg (McNicholas et al. 2011) and PyMOL (Schrödinger 2015).

Results

Gene synteny

In the Methanobacteria and Methanococci analyzed genomes *mtxX* is located adjacent to *uppS* that encodes undecaprenyl pyrophosphate synthase (Fig. 1) (e.g. *M. thermautotrophicus* ΔH O26334 MTH_232) a key enzyme in the biosynthesis of the undecaprenyl pyrophosphate lipid carrier for cell wall biosynthesis (Apfel et al. 1999). Recently, the cell wall biosynthesis enzymes for pseudomurein in Methanobacteria were analyzed (Subedi et al. 2021) with *uppS* found to be widely present in archaea. For Methanocaldococcus genomes *mtxX* is adjacent to *mmp12* Methanogen Marker Protein 12 (Fig. 1). Within Methanomicrobia, *mtxX* is adjacent to *mmp2* Methanogen Marker Protein 2 for Methanomicrobiales and Methanotrichales, but not for Methanosarcinales and Methanocellales (Fig. 2). *mmp2* is typically associated with genes encoding other MMPs in a large cluster (MMPs-2, 3, 5, 6, 15, and 17) (Woermann 2015). The clustering of *mtxX* with *mtxA* and *mtxH* (Harms and Thauer 1997, Wang et al. 2015) is observed for Methanosarcina, Methanohalophilus, and Methanococcoides (Fig. 2), but not for other methanogen genomes (Fig. 1 and Fig. 2).

MtxX tertiary and quaternary structure

The MtxX structure (242 amino acids) is an α/β fold comprising two subdomains (Fig. 3). The two MtxX molecules in the asymmetric unit form a dimer (Fig. 4) with 2376 Å^2 of their surface area buried at the dimer interface as determined by PISA (Krissinel and Henrick 2007). Comparison of the two monomers within the dimer shows the structures to be similar with RMSD 0.53 Å for the superposition of 226 Cα atoms. MtxX contains a prominent cleft in its

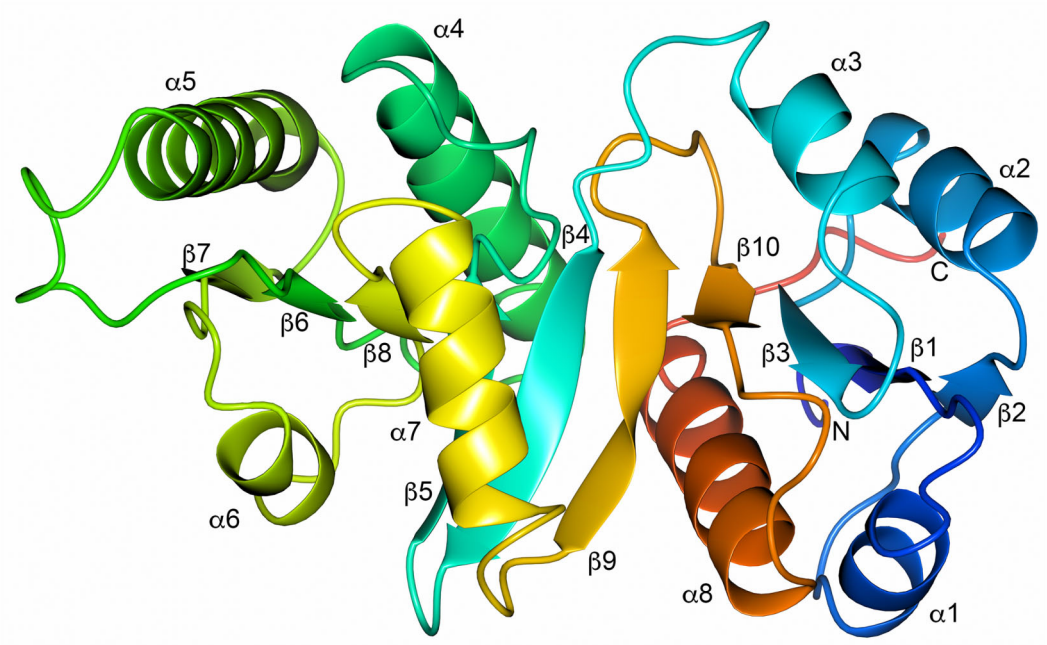

Figure 3 Cartoon representation of the MtxX tertiary structure colour-ramped N to C-terminus blue to red.

structure (Fig. 4) that is primarily formed between the two subdomains of a monomer, and with contributions to its structure from the non-crystallographically related monomer.

Multiple sequence alignment using MUSCLE (Edgar 2004) and Jalview (Waterhouse et al. 2009) shows that several amino acids lining the cleft, and residues at the dimer interface, are conserved (Fig. 5). This conservation of the dimer interface, the large, buried surface area and the binding clefts being formed from both monomers suggest that MtxX is a functional dimer. The cleft of one *Mth*MtxX monomer (monomer A) is occupied by the C-terminal residues 238–242 of a crystallographic symmetry-related (−X, Y+1/2, −Z) MtxX molecule (Fig. 4). ConSurf (Landau et al. 2005) analysis of orthologous MtxX sequences mapped onto the *Mth*MtxX structure (Fig. 6) shows that this cleft is the most conserved accessible surface and hence the most likely location for a functional site. Amino acids 238'-242' from the symmetry-related C-terminus form interactions with conserved residues within the binding cleft (amino acid numbering of the symmetry-related C-terminus is indicated by the addition of '). R54 contacts D240'; R74, N185 and R189 contact E242' (Fig. 4) while R216 interacts with D240' and N238'. R128(B), from monomer B, binds D240' and R134(B) contacts E242'. The conserved D213 (DTSR motif, Fig. 5) in the cleft interacts with N241'. S215 occupies an unusual sidechain rotamer (X_1=117°) interacting with S217 in a ST-turn (Duddy et al. 2004). The cleft also contains a bound ethylene glycol molecule from the cryoprotectant solution.

Comparison of the *Mth*MtxX structure to homologous structures

Structural homology searches with Foldseek (van Kempen et al. 2024) and Dali (Holm and Laakso 2016) against the RCSB Protein Data Bank (PDB) show that MtxX is homologous to phosphate acetyl/butyryltransferase domains (PTA/PTB EC 2.3.1.8/2.3.1.19) including the non-catalytic C-terminal PTA domain of MaeB hybrid malic enzymes (Harding et al. 2021) (Table 2). There is weaker homology (by Foldseek E-value and Dali Z-score) to NAD(P)-dependent decarboxylating dehydrogenases such as PdxA D-threonate 4-phosphate dehydrogenases, *cis*-dihydrodiol dehydrogenases, isocitrate, and propylmalate dehydrogenases. *Mth*MtxX is a smaller protein by between 30 and 100 amino acids compared to PTA and dehydrogenase sequences with most of the absent sequences being in subdomain 1 (Figs. 5 and 7). Analysis with Foldseek multimer (Kim et al. 2025) showed the MtxX dimerization mode is shared with homologous PTA (Fig. 7) and dehydrogenase structures, including as dimeric units within hexameric MaeB (Harding et al. 2021). Significant structural homology to methyltransferases is not detected.

MtxX S215, of the DTSR conserved sequence motif, is in the binding cleft (Fig. 4) where it is equivalently positioned to a conserved serine in the active site of PTA enzymes (Fig. 5). Superposition of the *Methanosarcina thermophila* PTA (*Mst*PTA) structure (Fig. 7) [PDB: 2AF4 (Lawrence et al. 2006)], aligns the catalytic S309 [also *Porphyromonas gingivalis* PTA (*Pg*PTA) S311, PDB: 6IOX (Yoshida et al. 2019) and *Treponema pallidum Tp*PTA S314, PDB: 8FIR (Brautigam et al. 2023)] onto *Mth*MtxX S215. The hypothesis that the *Mth*MtxX symmetry related C-terminus could be mimicking a functional MtxX binding interaction is strengthened by homology analysis showing that the bound symmetry-related D240' occupies an equivalent site in the *Mth*MtxX cleft (Fig. 7) as acetyl phosphate does in *Bacillus subtilis* PTA (Xu et al. 2005) and the coenzyme A (CoA) 3 phosphate for *Listeria monocytogenes* PTA (*Lm*PTA, PDB: 3U9E), and Asn241' occupies the same location in MtxX as the CoA ribose in *Lm*PTA and *Mst*PTA (Lawrence et al. 2006). There is heterogeneity of CoA and acetyl-CoA binding to orthologous PTAs (Fig. 7) meaning that a detailed superposition is not possible.

Other MtxX binding cleft residues are conserved with PTA active site residues (Fig. 5), but there are also differences. MtxX R216 is the equivalent residue to the PTA essential catalytic arginine

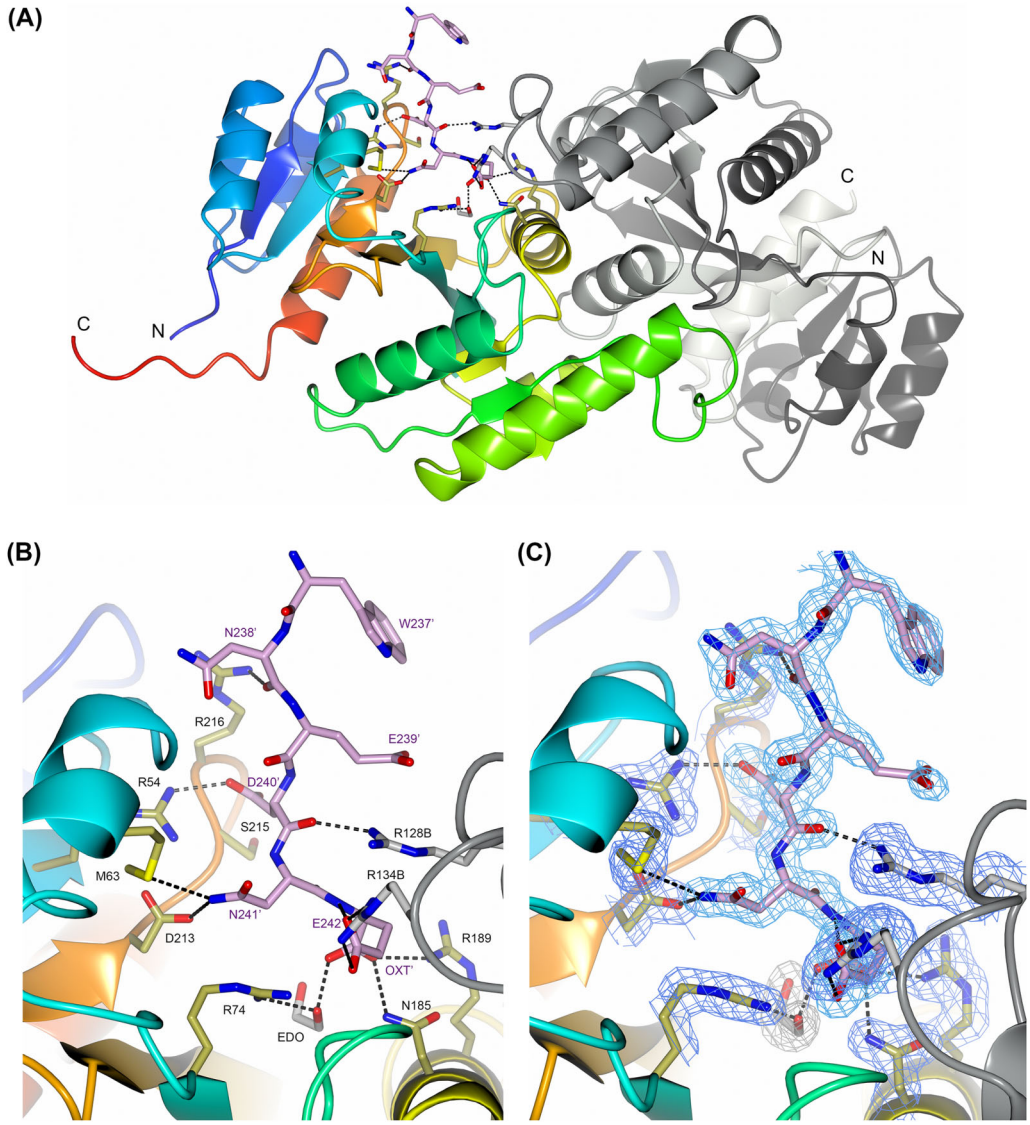

Figure 4 (A) Structure of dimeric MtxX colour-ramped N to C terminus; monomer A blue to red, and monomer B black to ivory. Residues 237'–242' of symmetry-related MtxX bound in the monomer A cleft are shown in stick representation (carbon pink, oxygen red, nitrogen blue). Selected amino acid side chains (4 Å neighbourhood) are shown with carbons coloured gold for monomer A and grey for monomer B. A bound ethylene glycol molecule (EDO) is shown. Hydrogen bonding interactions between molecules are indicated by dashed lines. (B) Close up view of symmetry-related MtxX 237–242 (pink) and neighbouring residues (gold/grey) in the cleft. (C) Electron density map (1 σ) contoured around symmetry-related 237'–242' (light blue), ethylene glycol (grey) and neighbouring residues (royal blue).

(e.g. *Mst*PTA R310, *Pg*PTA R312, *Tp*PTA R315) (Lawrence et al. 2006, Brautigam et al. 2023). On the other hand, the conserved PTA aspartate (e.g. *Mst*PTA D316, *Pg*PTA D318, *Tp*PTA D321) (Iyer et al. 2004) that has been proposed to act as the catalytic base in the acetyl transfer mechanism (Lawrence et al. 2006) is not conserved for MtxX (Fig. 5). The MtxX arginines R74, R128, R134 within the cleft that contact the acidic symmetry-related C-terminus are not conserved in PTAs possibly implying divergent functions.

Despite some overall structural similarity (Table 2) to dehydrogenase families, MtxX does not have histidines available to coordinate a metal ion as observed for the PdxA family (Sivaraman et al. 2003), and compared to IDH sequences MtxX lacks homologous regions of the 'NADP-binding' and 'phosphorylation' loops (Goncalves et al. 2012). For MtxX, the presence of its conserved cleft, and the fact that it is the substrate/ligand binding site in structural homologues suggests that the symmetry-related C-terminal tail binding mode observed for MtxX is mimicking a ligand interaction. The binding of the acidic C-terminal tail, the predominance of basic residues and the presence of the conserved hydrophobic amino acids F188 and L193 in the MtxX binding cleft suggests any native ligand for MtxX likely has hydrophobic as well as acidic character.

Discussion

The high-resolution crystal structure of methanogen *M. thermautotrophicus* ΔH MtxX has revealed a dimeric structure with a fold homologous to that of phosphate acetyltransferases and decarboxylating dehydrogenases with the identification of the po-

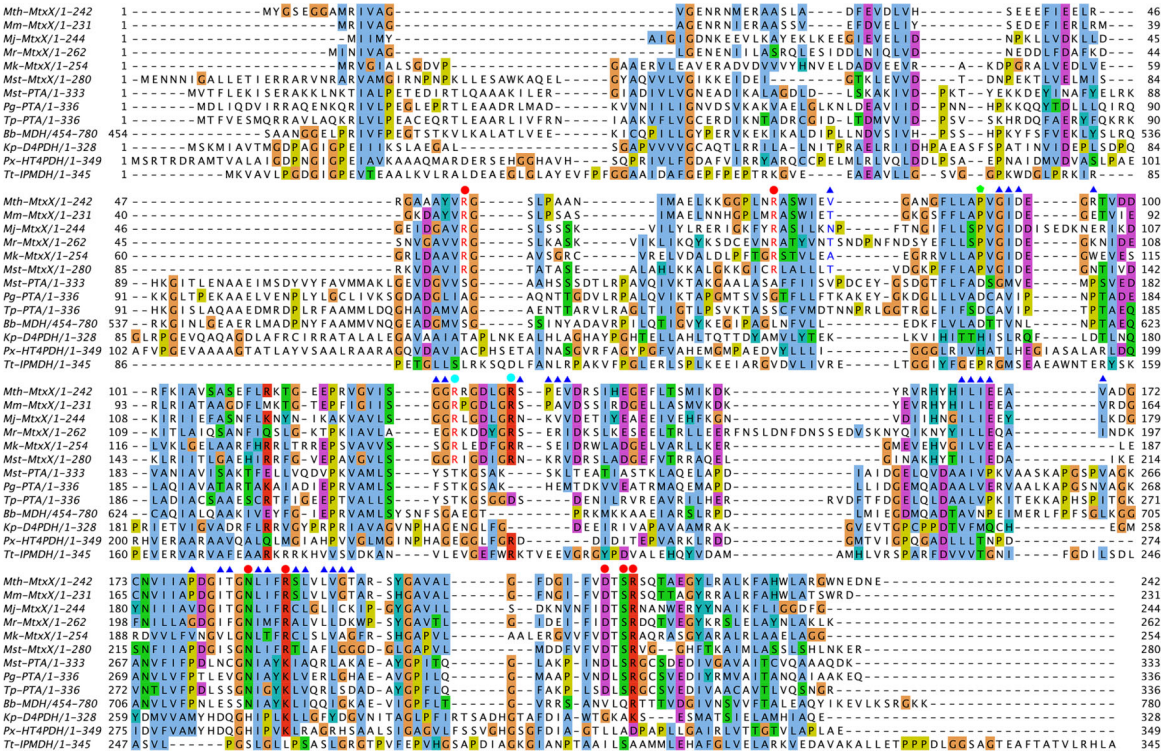

Figure 5 Multiple sequence alignment of MtxX proteins from *Methanothermobacter thermautotrophicus* ΔH (*Mth-MtxX*, O26333), *Methanothermobacter marburgensis* (*Mm-MtxX*, WP_013 295 499), *Methanocaldococcus jannaschii* (*Mj-MtxX*, Q58766), *Methanobrevibacter ruminantium* (*Mr-MtxX*, WP_012 955 805), *Methanopyrus kandleri* (*Mk-MtxX*, Q8TWU1), and *Methanosarcina thermophila* (*Mst-MtxX*, WP_048 166 052), phosphate acetyltransferases (PTA) from *M. thermophila* (*Mst-PTA*, P38503, PDB: 2AF4/1QZT), *Porphyromonas gingivalis* (*Pg-PTA*, B2RK03_PORG3, PDB: 6IOX) and *Treponema pallidum* (*Tp-PTA* O83132, PDB: 8FIR), and *Bdellovibrio bacteriovorus* malic enzyme MaeB PTA domain (*Bb-MDH*, WP_080 701 372, PDB: 6ZNT), *Klebsiella pneumoniae* D-threonate 4-phosphate dehydrogenase (*Kp-D4PDH*, A0A1Y0PY16_KLEPN, PDB: 6E85), *Paraburkholderia xenovorans* dehydrogenase (*Px-HT4PDH*, RP4_PARXL, PDB: 4ATY) and *Thermus thermophilus* isopropylmalate dehydrogenase (*Tt-IPMDH*, 3_THET8, PDB: 1OSJ). The alignment is coloured in the ClustalX (Larkin et al. 2007) scheme. Conserved *Mth-MtxX* amino acids located in the large cleft are labelled with a red circle, or a cyan circle if they are provided by the other monomer within the dimer (e.g. R128, R134). Additional residues involved in dimerization are labelled with a blue triangle. *Mth-MtxX* cis-proline 89 is indicated with a green circle. The multiple sequence alignment was calculated using MUSCLE (Edgar 2004) and displayed with Jalview (Waterhouse et al. 2009).

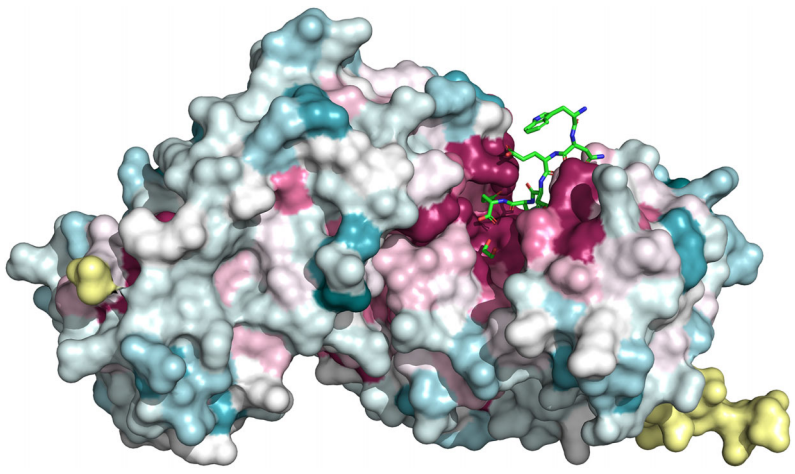

Figure 6 MtxX dimer surface representation coloured by sequence conservation calculated by ConSurf (Landau et al. 2005) (colour ramped from purple most conserved to cyan least conserved; yellow indicates insufficient data). The view is an approximately 180° rotation about the vertical axis from the view in Fig. 4 enabling the symmetry-related MtxX C-terminus and ethylene glycol (shown in stick representation with atomic colouring carbon green, oxygen red, nitrogen blue) to be visualized in the conserved cleft. The MtxX C-terminus (right hand side) is coloured yellow owing to a nonreliable conservation score.

Table 2 Foldseek analysis of MtxX structural homologues.

Homologous structure	E value	Score	Identical residues (%)	Enzyme	Coenzyme / substrate / ligand	Organism
1YCO	7.7×10^{-11}	304	20	Branched chain phosphotransacylase	Phosphate	*Enterococcus faecalis V583*
3U9E (3UF6)	1.7×10^{-10}	282	15	Putative phosphate acetyl/butyryl transferase	3U9E; CoA, 3UF6; CoD	*Listeria monocytogenes*
7T88	6.7×10^{-10}	272	14	Phosphate acetyltransferase		*Escherichia coli*
7VG9	8.1×10^{-10}	262	15	Phosphotransbutyrylase (Kim and Kim 2021)		*Clostridium acetobutylicum*
6ZNE (6ZNT)	2.6×10^{-9}	243	18	Malic enzyme (MaeB) (Harding et al. 2021)	6ZNT; CoA	*Bdellovibrio bacteriovorus*
1VMI	1.9×10^{-9}	240	17	Phosphate acetyltransferase (EutD)		*Escherichia coli*
6IOW(X)	1.4×10^{-8}	222	14	Phosphotransacetylase (Yoshida et al. 2019)	Acetyl-CoA	*Porphyromonas gingivalis*
8FIR	3.8×10^{-9}	213	19	Phosphoacyltransferase (PlsX); (Brautigam et al. 2023)		*Treponema pallidum*
1VIl	3.8×10^{-9}	206	15	Phosphoacyltransferase (PlsX) (Badger et al. 2005)		*Bacillus subtilis*
1QZT (2AF4)	2.9×10^{-7}	191	17	Phosphotransacetylase (Iyer et al. 2004)	2AF4; CoA	*Methanosarcina thermophila*
6E85	4.5×10^{-7}	175	11	D-threonate 4-phosphate dehydrogenase (PdxA); (Inniss et al. 2023)	Ni, POP	*Klebsiella pneumoniae ST23*
4ATY	4.5×10^{-7}	170	13	Terephthalate 1,2-*cis*-dihydrodiol dehydrogenase (PdxA) (Bains et al. 2012)	Zn	*Burkholderia xenovorans LB400*
8GS5	6.9×10^{-7}	163	11	Isocitrate dehydrogenase (Chen et al. 2022)		*Homo sapiens*
5HN3	5.1×10^{-7}	156	14	Isocitrate dehydrogenase (Shimizu et al. 2017)	Mn, Isocitrate	*Thermococcus kodakarensis*
2Y3Z (1OSJ)	3.4×10^{-5}	127	12	Isopropylmalate dehydrogenase (Ma and Yun 2018)		*Thermus thermophilus*

Abbreviations; CoA coenzyme A, CoD 3-dephosphocoenzyme A, POP pyrophosphate.

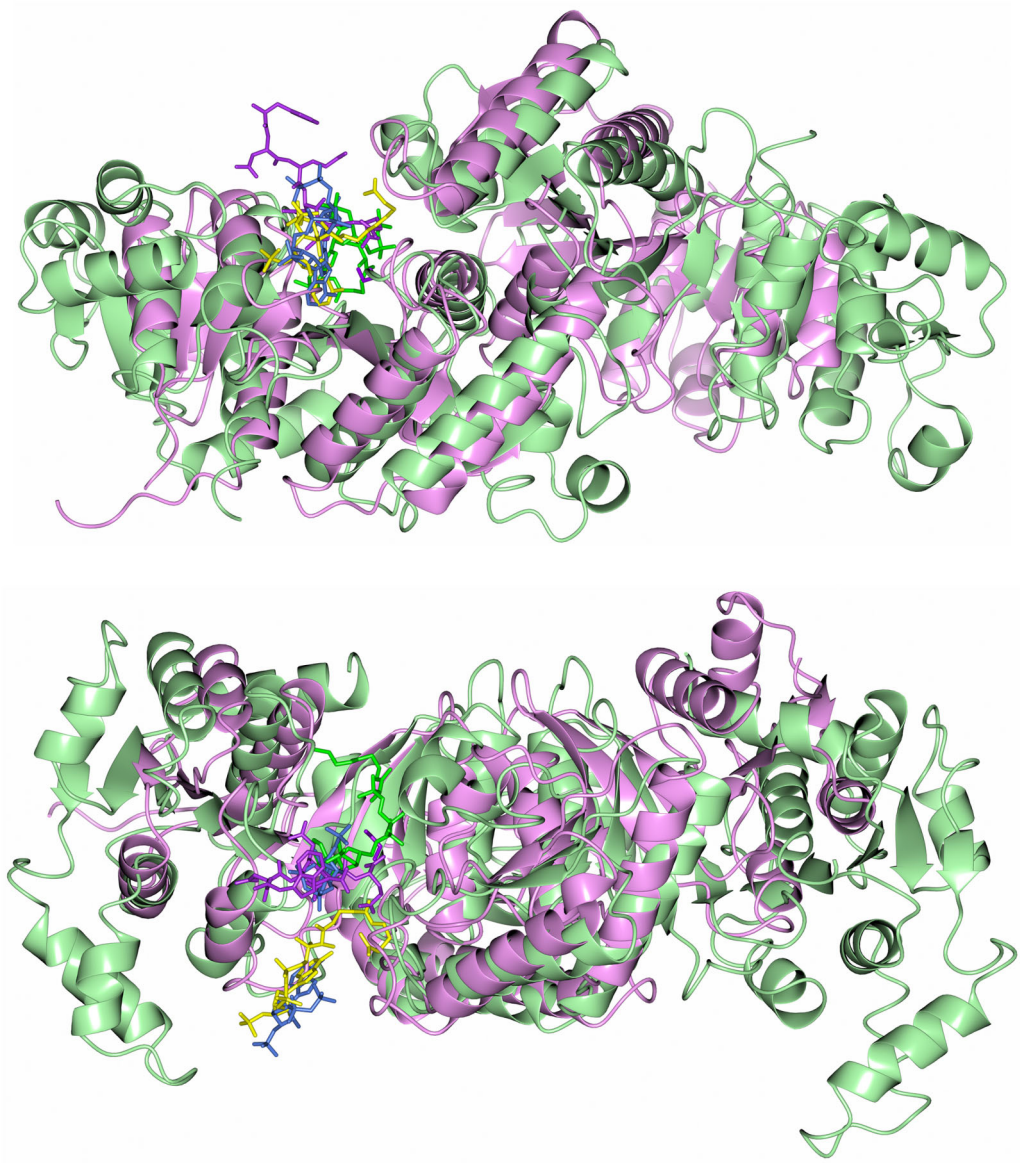

Figure 7 Approximately orthogonal views of the superposition of MtxX and phosphate acetyltransferase (PTA) structures including bound coenzyme A (CoA) or acetyl-coenzyme A (acetyl-CoA). MtxX (cartoon representation), the C-terminus of symmetry-related MtxX and the ethylene glycol molecule (both stick representation) bound in the MtxX cleft are coloured violet. *Methanosarcina thermophila* PTA (2AF4, cartoon representation) with coenzyme A (stick representation) bound (Lawrence et al. 2006) is coloured green; the root mean square difference (RSMD) is 3.1 Å for the superposition of 213 Ca atoms with MtxX. *Listeria monocytogenes* PTA (3U9E) bound coenzyme A is shown in blue stick representation; RSMD is 2.4 Å for the superposition of 207 Ca with MtxX (PTA is not shown for clarity). *Porphyromonas gingivalis* PTA (6IOX) bound acetyl-CoA (Yoshida et al. 2019) is coloured yellow; RSMD is 3.0 Å for the superposition of 206 Ca with MtxX (PTA is not shown for clarity). CoA and acetyl-CoA are shown for a single PTA monomer. Superpositions were performed on MtxX monomer A. The upper view is approximately the same orientation as Fig. 4, the lower view is rotated ∼90° about the horizontal axis.

tential binding/functional site cleft. *Mth*MtxX amino acids from both monomers contribute to the two conserved clefts within the dimer. In the crystal structure, the cleft of one monomer (monomer A) binds the acidic C-terminus of a crystallographic symmetry-related MtxX molecule giving some indication of the binding properties of this site with conserved, predominantly basic, residues in the cleft interacting with the crystallographic acidic C-terminus. The *Mth*MtxX C-terminus is not conserved for MtxX sequences from other methanogens (Fig. 5) so this binding likely does not represent a functional or regulatory interaction but does serve to highlight the conserved binding cleft and interaction mode that might mimic that of the MtxX native binding ligand. The MtxX binding site is located similarly to the active site of phosphate acetyltransferases. PTAs catalyse the reversible transfer of the acetyl group from acetyl phosphate to CoA to produce acetyl-CoA and inorganic phosphate. Within methanogens, PTAs have been annotated only for the acetoclastic *Methanosarcina* where they function in concert with acetate kinase producing acetyl-CoA from acetate (Fournier and Gogarten 2008, Gilmore et al. 2017); the presence of these two genes in *Methanosarcina* is a result of horizontal gene transfer from bacteria (Fournier and Gogarten 2008). PTA genes and activity have not been described for hydrogenotrophic CO_2 reducing methanogens such as *M. thermautotrophicus* ΔH. For example, *Methanocal-*

dococcus jannaschii has MtxX and does not exhibit phosphate acetyltransferase, or acetyl-CoA synthetase activity (Sprott et al. 1993).

The presence of *mtxX* within a methyltransferase-related *mtxXAH* operon for some methanogen genomes had led to the annotation of MtxX as a methyltransferase, however gene synteny analysis shows that *mtxX* clustering with *mtxA* and *mtxH* only occurs for a subset of methanogen orders and is not typical amongst methanogen genomes. The MtxX protein structure has the highest homology to phosphate acetyltransferases and not methyltransferases. However, this structural homology does not rule out a role for MtxX in methyl group transfer processes and/or the biochemistry of specialized methanogenic archaeal processes. Further genetic and biochemical characterization of MtxX activity is required, as is the establishment of a functional assay to identify ligand molecules.

Acknowledgements

We appreciate support from the Australian Synchrotron in Melbourne and the New Zealand Synchrotron Group. This research was undertaken in part using the MX1 and MX2 beamlines at the Australian Synchrotron, part of ANSTO, and made use of the Australian Cancer Research Foundation (ACRF) detector. We thank the Pastoral Greenhouse Gas Research Consortium (PGgRc) and manager Mark Aspin for their support. We thank Graeme Attwood and Nikola Palevich for helpful feedback on the manuscript.

Author contribution

AJSS, VC, LRS, WKC, MW, and RSR were responsible for the experimental design, and conducted the experimental analysis. AJSS, VC, LRS, and RSR drafted and revised the manuscript.

Supplementary material

Supplementary material is available at *FEMSMC Journal* online.

Conflicts of interest

None declared.

Funding

Pastoral Greenhouse Gas Research Consortium (PGgRc), New Zealand Synchrotron Group, Australian Synchrotron (ANSTO).

References

Adam PS, Kolyfetis GE, Bornemann TLV *et al.* Genomic remnants of ancestral methanogenesis and hydrogenotrophy in Archaea drive anaerobic carbon cycling. *Sci Adv* 2022;**8**:eabm9651. https://doi.org/10.1126/sciadv.abm9651.

Adler SA, Chadwick GL, Nayak DD. Assembly and maturation of methyl-coenzyme M reductase in methanogenic archaea. *Curr Opin Microbiol* 2025;**87**:102637. https://doi.org/10.1016/j.mib.2025.102637.

Apfel CM, Takacs B, Fountoulakis M *et al.* Use of genomics to identify bacterial undecaprenyl pyrophosphate synthetase: cloning, expression, and characterization of the essential uppS gene. *J Bacteriol* 1999;**181**:483–92. https://doi.org/10.1128/JB.181.2.483-492.1999.

Aragao D, Aishima J, Cherukuvada H *et al.* MX2: a high-flux undulator microfocus beamline serving both the chemical and macromolecular crystallography communities at the Australian Synchrotron. *J Synchrotron Rad* 2018;**25**:885–91. https://doi.org/10.1107/S1600577518003120.

Badger J, Sauder JM, Adams JM *et al.* Structural analysis of a set of proteins resulting from a bacterial genomics project. *Proteins* 2005;**60**:787–96. https://doi.org/10.1002/prot.20541.

Bains J, Wulff JE, Boulanger MJ. Investigating terephthalate biodegradation: structural characterization of a putative decarboxylating cis-dihydrodiol dehydrogenase. *J Mol Biol* 2012;**423**:284–93. https://doi.org/10.1016/j.jmb.2012.07.022.

Basu MK, Selengut JD, Haft DH. ProPhylo: partial phylogenetic profiling to guide protein family construction and assignment of biological process. *BMC Bioinf* 2011;**12**:434. https://doi.org/10.1186/1471-2105-12-434.

Borrel G, Adam PS, McKay LJ *et al.* Wide diversity of methane and short-chain alkane metabolisms in uncultured archaea. *Nat Microbiol* 2019;**4**:603–13. https://doi.org/10.1038/s41564-019-0363-3.

Borrel G, Parisot N, Harris HM *et al.* Comparative genomics highlights the unique biology of Methanomassiliicoccales, a Thermoplasmatales-related seventh order of methanogenic archaea that encodes pyrrolysine. *BMC Genomics* 2014;**15**:679. https://doi.org/10.1186/1471-2164-15-679.

Brautigam CA, Deka RK, Tso SC *et al.* Biophysical and biochemical studies support TP0094 as a phosphotransacetylase in an acetogenic energy-conservation pathway in *Treponema pallidum*. *PLoS One* 2023;**18**:e0283952. https://doi.org/10.1371/journal.pone.0283952.

Chen X, Sun P, Liu Y *et al.*. Structures of a constitutively active mutant of human IDH3 reveal new insights into the mechanisms of allosteric activation and the catalytic reaction. *J Biol Chem* 2022;**298**:102695. https://doi.org/10.1016/j.jbc.2022.102695.

Cowieson NP, Aragao D, Clift M *et al.* MX1: a bending-magnet crystallography beamline serving both chemical and macromolecular crystallography communities at the Australian Synchrotron. *J Synchrotron Rad* 2015;**22**:187–90. https://doi.org/10.1107/S1600577514021717.

Cowtan K. The Buccaneer software for automated model building. 1. Tracing protein chains. *Acta Crystallogr D Biol Crystallogr* 2006;**62**:1002–11. https://doi.org/10.1107/S0907444906022116.

Davis IW, Murray LW, Richardson JS *et al.* MOLPROBITY: structure validation and all-atom contact analysis for nucleic acids and their complexes. *Nucleic Acids Res* 2004;**32**:W615–9. https://doi.org/10.1093/nar/gkh398.

Duddy WJ, Nissink JW, Allen FH *et al.* Mimicry by asx- and ST-turns of the four main types of beta-turn in proteins. *Protein Sci* 2004;**13**:3051–5. https://doi.org/10.1110/ps.04920904.

Edgar RC. MUSCLE: multiple sequence alignment with high accuracy and high throughput. *Nucleic Acids Res* 2004;**32**:1792–7. https://doi.org/10.1093/nar/gkh340.

Emsley P, Cowtan K. Coot: model-building tools for molecular graphics. *Acta Crystallogr D Biol Crystallogr* 2004;**60**:2126–32. https://doi.org/10.1107/S0907444904019158.

Evans PR, Murshudov GN. How good are my data and what is the resolution? *Acta Crystallogr D Biol Crystallogr* 2013;**69**:1204–14. https://doi.org/10.1107/S0907444913000061.

Evans PR. An introduction to data reduction: space-group determination, scaling and intensity statistics. *Acta Crystallogr D Biol Crystallogr* 2011;**67**:282–92. https://doi.org/10.1107/S090744491003982X.

Federhen S. The NCBI Taxonomy database. *Nucleic Acids Res* 2012;**40**:D136–43. https://doi.org/10.1093/nar/gkr1178.

Fournier GP, Gogarten JP. Evolution of acetoclastic methanogenesis in Methanosarcina via horizontal gene transfer from cellulolytic Clostridia. *J Bacteriol* 2008;**190**:1124–7. https://doi.org/10.1128/JB.01382-07.

Gao B, Gupta RS. Phylogenomic analysis of proteins that are distinctive of Archaea and its main subgroups and the origin of methanogenesis. *BMC Genomics* 2007;**8**:86. https://doi.org/10.1186/1471-2164-8-86.

Gilmore SP, Henske JK, Sexton JA *et al.* Genomic analysis of methanogenic archaea reveals a shift towards energy conservation. *BMC Genomics* 2017;**18**:639. https://doi.org/10.1186/s12864-017-4036-4.

Goncalves S, Miller SP, Carrondo MA *et al.* Induced fit and the catalytic mechanism of isocitrate dehydrogenase. *Biochemistry* 2012;**51**:7098–115. https://doi.org/10.1021/bi300483w.

Harding CJ, Cadby IT, Moynihan PJ *et al.* A rotary mechanism for allostery in bacterial hybrid malic enzymes. *Nat Commun* 2021;**12**:1228. https://doi.org/10.1038/s41467-021-21528-2.

Harms U, Thauer RK. Identification of the active site histidine in the corrinoid protein MtrA of the energy-conserving methyltransferase complex from *Methanobacterium thermoautotrophicum*. *Eur J Biochem* 1997;**250**:783–8. https://doi.org/10.1111/j.1432-1033.1997.00783.x.

Harms U, Weiss DS, Gartner P *et al.* The energy conserving N5-methyltetrahydromethanopterin:coenzyme M methyltransferase complex from *Methanobacterium thermoautotrophicum* is composed of eight different subunits. *Eur J Biochem* 1995;**228**:640–8. https://doi.org/10.1111/j.1432-1033.1995.0640m.x.

Holm L, Laakso LM. Dali server update. *Nucleic Acids Res* 2016;**44**:W351–5. https://doi.org/10.1093/nar/gkw357.

Inniss NL, Kochan TJ, Minasov G *et al.*. A structural systems biology approach to high-risk CG23 *Klebsiella pneumoniae*. *Microbiol Resour Announc* 2023;**12**:e0101322. https://doi.org/10.1128/mra.01013-22.

Iyer PP, Lawrence SH, Luther KB *et al.* Crystal structure of phosphotransacetylase from the methanogenic archaeon *Methanosarcina thermophila*. *Structure* 2004;**12**:559–67. https://doi.org/10.1016/j.str.2004.03.007.

Kabsch W. XDS. *Acta Crystallogr D Biol Crystallogr* 2010;**66**:125–32. https://doi.org/10.1107/S0907444909047337.

Kaster AK, Goenrich M, Seedorf H *et al.* More than 200 genes required for methane formation from H_2 and CO_2 and energy conservation are present in *Methanothermobacter marburgensis* and *Methanothermobacter thermautotrophicus*. *Archaea* 2011;**2011**:1. https://doi.org/10.1155/2011/973848.

Kim S, Kim KJ. Crystal structure and molecular mechanism of phosphotransbutyrylase from *Clostridium acetobutylicum*. *J Microbiol Biotechnol* 2021;**31**:1393–400. https://doi.org/10.4014/jmb.2109.09036.

Kim W, Mirdita M, Levy Karin E *et al.* Rapid and sensitive protein complex alignment with Foldseek-Multimer. *Nat Methods* 2025;**22**:469–72. https://doi.org/10.1038/s41592-025-02593-7.

Krissinel E, Henrick K. Inference of macromolecular assemblies from crystalline state. *J Mol Biol* 2007;**372**:774–97. https://doi.org/10.1016/j.jmb.2007.05.022.

Landau M, Mayrose I, Rosenberg Y *et al.* ConSurf 2005: the projection of evolutionary conservation scores of residues on protein structures. *Nucleic Acids Res* 2005;**33**:W299–302. https://doi.org/10.1093/nar/gki370.

Larkin MA, Blackshields G, Brown NP *et al.* Clustal W and Clustal X version 2.0. *Bioinformatics* 2007;**23**:2947–8. https://doi.org/10.1093/bioinformatics/btm404.

Lawrence SH, Luther KB, Schindelin H *et al.* Structural and functional studies suggest a catalytic mechanism for the phosphotransacetylase from *Methanosarcina thermophila*. *J Bacteriol* 2006;**188**:1143–54. https://doi.org/10.1128/JB.188.3.1143-1154.2006.

Leahy SC, Kelly WJ, Altermann E *et al.* The genome sequence of the rumen methanogen *Methanobrevibacter ruminantium* reveals new possibilities for controlling ruminant methane emissions. *PLoS One* 2010;**5**:e8926. https://doi.org/10.1371/journal.pone.0008926.

Ma R, Yun CH. Crystal structures of pan-IDH inhibitor AG-881 in complex with mutant human IDH1 and IDH2. *Biochem Biophys Res Commun* 2018;**503**:2912–7. https://doi.org/10.1016/j.bbrc.2018.08.068.

McNicholas S, Potterton E, Wilson KS *et al.* Presenting your structures: the CCP4mg molecular-graphics software. *Acta Crystallogr D Biol Crystallogr* 2011;**67**:386–94. https://doi.org/10.1107/S0907444911007281.

Murshudov GN, Skubak P, Lebedev AA *et al.* REFMAC5 for the refinement of macromolecular crystal structures. *Acta Crystallogr D Biol Crystallogr* 2011;**67**:355–67. https://doi.org/10.1107/S0907444911001314.

Nobu MK, Narihiro T, Kuroda K *et al.* Chasing the elusive Euryarchaeota class WSA2: genomes reveal a uniquely fastidious methyl-reducing methanogen. *ISME J* 2016;**10**:2478–87. https://doi.org/10.1038/ismej.2016.33.

Oberto J. SyntTax: a web server linking synteny to prokaryotic taxonomy. *BMC Bioinf* 2013;**14**:4. https://doi.org/10.1186/1471-2105-14-4.

Sarmiento F, Mrazek J, Whitman WB. Genome-scale analysis of gene function in the hydrogenotrophic methanogenic archaeon *Methanococcus maripaludis*. *Proc Natl Acad Sci USA* 2013;**110**:4726–31. https://doi.org/10.1073/pnas.1220225110.

Schrödinger L. The PyMOL molecular graphics system version 3.1. 2015.

Sheldrick GM. Experimental phasing with SHELXC/D/E: combining chain tracing with density modification. *Acta Crystallogr D Biol Crystallogr* 2010;**66**:479–85. https://doi.org/10.1107/S0907444909038360.

Shimizu T, Yin L, Yoshida A *et al.*. Structure and function of an ancestral-type beta-decarboxylating dehydrogenase from *Thermococcus kodakarensis*. *Biochem J* 2017;**474**:105–22. https://doi.org/10.1042/BCJ20160699.

Shin DH. Preliminary structural studies on the MtxX protein from *Methanococcus jannaschii*. *Acta Crystallogr F Struct Biol Cryst Commun* 2008;**64**:300–3. https://doi.org/10.1107/S1744309108007033.

Sivaraman J, Li Y, Banks J *et al.* Crystal structure of *Escherichia coli* PdxA, an enzyme involved in the pyridoxal phosphate biosynthesis pathway. *J Biol Chem* 2003;**278**:43682–90. https://doi.org/10.1074/jbc.M306344200.

Skubak P, Pannu NS. Automatic protein structure solution from weak X-ray data. *Nat Commun* 2013;**4**:2777. https://doi.org/10.1038/ncomms3777.

Sprott GD, Ekiel I, Patel GB. Metabolic pathways in *Methanococcus jannaschii* and other methanogenic bacteria. *Appl Environ Microb* 1993;**59**:1092–8. https://doi.org/10.1128/aem.59.4.1092-1098.1993.

Subedi BP, Martin WF, Carbone V *et al.* Archaeal pseudomurein and bacterial murein cell wall biosynthesis share a common evolutionary ancestry. *FEMS Microbes* 2021;**2**:xtab012. https://doi.org/10.1093/femsmc/xtab012.

van Kempen M, Kim SS, Tumescheit C *et al.* Fast and accurate protein structure search with Foldseek. *Nat Biotechnol* 2024;**42**:243–6. https://doi.org/10.1038/s41587-023-01773-0.

Wang S, Chen Y, Cao Q *et al.* Long-lasting gene conversion shapes the convergent evolution of the critical methanogenesis genes. *G3* 2015;**5**:2475–86. https://doi.org/10.1534/g3.115.020180.

Waterhouse AM, Procter JB, Martin DM *et al.* Jalview Version 2–a multiple sequence alignment editor and analysis workbench. *Bioinformatics* 2009;**25**:1189–91. https://doi.org/10.1093/bioinformatics/btp033.

Winn MD, Ballard CC, Cowtan KD *et al.* Overview of the CCP4 suite and current developments. *Acta Crystallogr D Biol Crystallogr* 2011;**67**:235–42. https://doi.org/10.1107/S0907444910045749.

Winter G, Waterman DG, Parkhurst JM *et al.* DIALS: implementation and evaluation of a new integration package. *Acta Crystallogr D Struct Biol* 2018;**74**:85–97. https://doi.org/10.1107/S2059798317017235.

Woermann M. *Investigation of Methanogenesis Marker Proteins: implications for Environmental Processes*. MSc Thesis. University of Duisburg-Essen, 2015.

Xu QS, Jancarik J, Lou Y *et al.* Crystal structures of a phosphotransacetylase from *Bacillus subtilis* and its complex with acetyl phosphate. *J Struct Funct Genomics* 2005;**6**:269–79. https://doi.org/10.1007/s10969-005-9001-9.

Yoshida Y, Sato M, Nonaka T *et al.* Characterization of the phosphotransacetylase-acetate kinase pathway for ATP production in *Porphyromonas gingivalis*. *Journal of Oral Microbiology* 2019;**11**:1588086. https://doi.org/10.1080/20002297.2019.1588086.

Received: 11 September 2025. **Revised:** 10 February 2026. **Accepted:** 13 February 2026